

# SUMER observations of Doppler shift in the quiet Sun and in an active region

L. Teriaca<sup>1</sup>, D. Banerjee<sup>1</sup>, and J.G. Doyle<sup>1</sup>

Armagh Observatory, College Hill, Armagh BT61 9DG, Ireland (lte, dipu, jgd@star.arm.ac.uk)

Received 26 March 1999 / Accepted 21 June 1999

**Abstract.** The UV spectral lines formed at transition region temperatures in the solar atmosphere, show a prevailing redshifted emission. Using the Solar Ultraviolet Measurements of Emitted Radiation spectrometer flown on the *Solar and Heliospheric Observatory* spacecraft, we measure the amount of line shift as a function of the temperature for several spectral lines formed in the range between  $10^4$  and  $10^6$  K. We analyze spectrograms relative to the quiet Sun and to the active region NOAA 7946. The velocities derived are increasing from a redshift of  $\sim 0$  km s<sup>-1</sup> at  $\sim 20000$  K to  $10$  km s<sup>-1</sup> at  $1.9 \cdot 10^5$  K for the quiet Sun, and to  $\sim 15$  km s<sup>-1</sup> at  $10^5$  K for the active region. At higher temperature an opposite behaviour is observed. In the quiet Sun a *blueshift* of  $\sim -2$  km s<sup>-1</sup> is observed at the Ne VIII formation temperature ( $6.3 \cdot 10^5$  K), while in the active region, a *blue-shifted* value around  $-8$  km s<sup>-1</sup> is observed for the same spectral line. The finding of blueshift in Ne VIII is due to the adoption of a new rest wavelength of  $770.428$  Å. By  $10^6$  K the *blueshift* is  $\sim -10$  km s<sup>-1</sup> in the active region as measured by Fe XII 1242.

**Key words:** Sun: atmosphere – Sun: transition region – Sun: UV radiation

## 1. Introduction

One of the most interesting problems in solar physics is the observed redshifted emission of lines formed at transition region (TR) temperatures. During the last two decades, observations of this phenomenon were obtained by many authors using several UV instruments with different spatial resolution (see Brekke et al. 1997 and references therein). In earlier investigations the magnitude of the redshift has been found to increase with temperature, reaching a maximum (around  $8$  km s<sup>-1</sup> in the quiet Sun) at  $T = 10^5$  K, and then to decrease towards higher temperatures. Doschek et al. (1976) found no significant shift in the O V line at  $1218$  Å at disk center and the commonly quoted average velocity variation with temperature above  $10^5$  K depended to a large extent on this particular observation of the  $1218$  Å line. Chae et al. (1998a), have shown that, for the quiet Sun, the redshift is peaked around  $1.5 \cdot 10^5$  K with a value of

$11$  km s<sup>-1</sup> but it is also present at higher temperatures with a value around  $5$  km s<sup>-1</sup> for Ne VIII  $770.409$  Å in the quiet Sun. Similar results were also obtained by Brekke et al. (1997). Peter & Judge (1999) have found *blueshifts* at disk center for three coronal lines in the dataset Ne VIII at  $770$  Å and  $780$  Å and Mg X at  $625$  Å, in contradiction to the two previous papers but in agreement with an Fe XII  $1349.375$  Å measurement by Sandlin et al. (1977) based on SKYLAB data. This difference in the value of Doppler shift for the Ne VIII  $770$  line is due to the assumption of a new rest wavelength of  $770.428$  Å. More recently, this value for the Ne VIII rest wavelength has been confirmed by Dammasch et al., (1999). Peter (1999) and Peter & Judge (1999) found also, at spatial scales up to  $50$  arc sec, clear evidence of a center-to-limb redshift behaviour consistent with a  $\cos \theta$  behaviour in all transition region lines and a  $\cos \theta$  *blueshift* behaviour for the three upper transition region/coronal lines listed above. This suggests an explanation in term of prevalent vertical mass or wave motion for the observed line shift.

Transition region and coronal emission lines show a full width half maximum that can not be explained only with Doppler thermal broadening (Mariska, 1992). Motion associated with small and large scale motion and/or wave propagation can explain the observed broadening. For optically thick lines, opacity effects will contribute to the line broadening. However the majority of TR and coronal emission lines, such as Si IV, C IV, N V, S VI, O VI, Mg X, are optically thin and opacity effects can be ruled out at least for the quiet Sun (Chae et al., 1998b). In this case, after correcting for instrumental broadening, the measured full width half maximum can be written as,

$$FWHM = \left[ 4 \ln 2 \left( \frac{\lambda}{c} \right)^2 \left( \frac{2k_B T_i}{M} + \xi^2 \right) \right]^{1/2} \quad (1)$$

where  $M$  is the ion mass,  $\xi$  is the non-thermal speed and  $T_i$  is the ion temperature. At transition region densities and temperatures, the electrons and ions rapidly equilibrate (Mariska, 1992) and a single temperature plasma can be assumed at least for on-disk measurements.  $\xi$  is an indication of the amount of turbulence and/or waves present in the plasma at a certain temperature and can be useful to discriminate between different theoretical models. Chae et al. (1998b) using SUMER observations, shows a de-

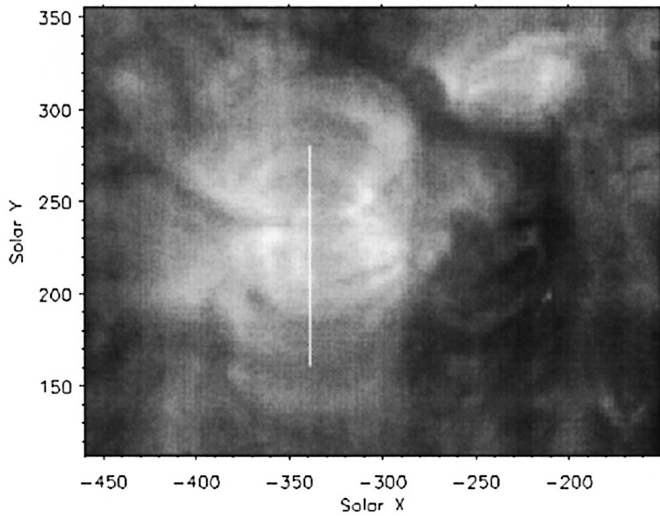


**Fig. 1.** Slit location in Active Region NOAA 7946 (23 February 1996) on an EIT images in Fe IX-X (courtesy of the EIT consortium).

pendence of  $\xi$  with temperature, from  $\sim 5 \text{ km s}^{-1}$  at  $1.5 \cdot 10^4 \text{ K}$ , reaching a maximum of  $\sim 30 \text{ km s}^{-1}$  at  $3 \cdot 10^5 \text{ K}$  and returning down to  $\sim 18 \text{ km s}^{-1}$  at  $10^6 \text{ K}$ . Similar trends were also detected previously by other authors and a review can be found in Mariska (1992). In this paper we present measurements of Doppler shift and non-thermal velocity of TR and coronal lines for Active Region NOAA 7946 and for the quiet Sun at disk center. The extremely good quality of the active region dataset and the particular location of the slit, which is placed between the two regions of opposite polarity, allows us to give a new insight into the problem of observed line shift in the solar TR and corona.

## 2. Observations

SUMER is a normal incidence spectrograph operating over the wavelength range  $450 \text{ \AA}$  to  $1610 \text{ \AA}$ . It is a powerful UV instrument capable of making reliable measurements of bulk motions in the chromosphere, transition region and low corona with a spectral resolution of  $45 \text{ m\AA/pix}$  at  $800 \text{ \AA}$  (first order) and a spatial resolution of 1 arcsec across and 2 arcsec along the slit (Wilhelm et al. 1995; Lemaire et al. 1997). Four slits are available;  $4 \times 300$ ,  $1 \times 300$ ,  $1 \times 120$  and  $0.3 \times 120 \text{ arcsec}^2$ . The detectors (see Siegmund et al., 1994) have 1024 spectral pixels and 360 spatial pixels, each. The central area is coated with KBr which increases the quantum efficiency by up to an order of magnitude in the range  $900 \text{ \AA}$  to  $1500 \text{ \AA}$ .

The observations discussed were obtained in Feb. '96 and consist of a series of spectral images covering the wavelength range between  $800$  and  $1590 \text{ \AA}$ . Every spectrum is partially overlapping the previous and the following, in order to ensure that the spectral lines are recorded on both the bare and the KBr parts of the detector. This allows us to recognize the second order lines from the first order ones using the different wavelength-dependent sensitivity of KBr compared to the bare part. During Feb. '96 the Sun was at the minimum of the sunspot cycle, with

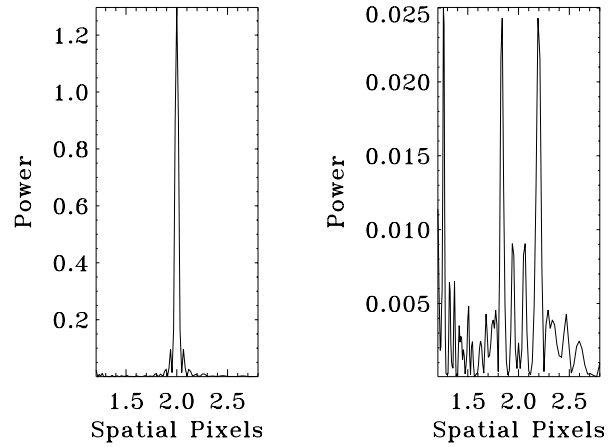


**Fig. 2.** Power spectrum of the average along the slit of an image relative to the Quiet Sun before (*left panel*) and after (*right panel*) the flat field subtraction, showing the reduction in the electronic modulation.

very few active regions present on the disk (see Fig. 1). The two datasets (for the active region and for the QS) consist of a series of spectra characterized by the same reference pixel-wavelength (with the exclusion of 4 spectra in the QS that do not have a correspondence in the AR). Every single spectrum was exposed for 100 seconds using the  $1 \times 120$  slit in the quiet Sun and in Active Region NOAA 7946 for a total of 41 and 37 spectra respectively. The dates of observations, locations, pointing, slit size and exposure times are given in Table 1.

## 3. Data reduction

Reduction of SUMER raw images follow several stages, i.e. dead time correction, local gain correction, flat field subtraction, radiometric calibration (in order to pass from  $\text{count px}^{-1} \text{ s}^{-1}$  to  $\text{erg cm}^{-2} \text{ s}^{-1} \text{ Sr}^{-1} \text{ \AA}^{-1}$ ) and a correction for geometrical distortion. All these stages were applied to our data.

### 3.1. Dead time and local gain corrections

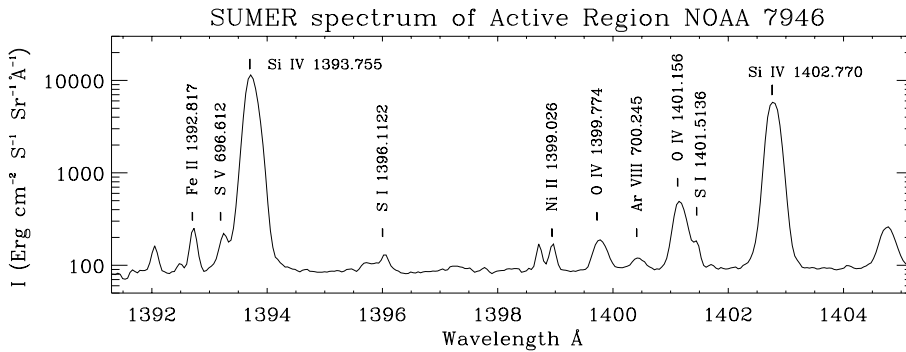
For a total counting rate up to  $5 \cdot 10^4 \text{ events s}^{-1}$ , a correction for the dead-time effect needs to be applied (Wilhelm et al. 1995; Hollandt et al. 1996). Another, more serious, effect arises when for certain bright lines (i.e. C III  $977 \text{ \AA}$  or O VI  $1032 \text{ \AA}$ ) levels up to  $10 \text{ counts pix}^{-1} \text{ s}^{-1}$  are reached. In these cases a local reduction in the micro channel plate (MCP) gain and, therefore, a loss of dynamic range will be present for such strong lines (Wilhelm et al., 1997). In these cases also a correction for the local gain depression needs to be applied. These two corrections must be applied at the initial stage.

### 3.2. Flat field subtraction

Flat field subtraction is necessary in order to correct for non uniformity in the sensitivity of the detector on scales of about 20 pixels or less. Flat field images are taken approximately every month with a  $\sim 3$  hour exposure in the Lyman continuum

**Table 1.** SUMER observations of Active Region NOAA 7946 and Quiet Sun (QS). Slit 4 = 1x120 arcsec<sup>2</sup>.

Date	Region	Detector	Slit	Solar X-Y	Observing period	No. of spectra	Wavelength range (Å)
23 Feb'96	NOAA 7946	A	4	-364,+219	19:11-19:44	18	1252-1592
23 Feb'96	NOAA 7946	A	4	-359,+219	19:44-20:27	19	786-1275
23 Feb'96	Quiet Sun	A	4	+1,0	21:34-22:12	20	1158-1592
23 Feb'96	Quiet Sun	A	4	+7,0	22:12-22:30	10	980-1180
23 Feb'96	Quiet Sun	A	4	+10,0	22:30-22:50	11	786-1002

**Fig. 3.** SUMER spectrum of Active Region NOAA 7946.

between 860 and 900 Å while the spectrometer grating is defocused (Wilhelm et al., 1997). In some cases the flat field was subtracted on-board using the last acquired image. In our dataset this is the case for the data related to the active region NOAA 7946. The flat field correction also eliminates or, at least greatly reduces, a modulation of approximately 20% every two pixels in the spatial dimension caused by an analogue-to-digital converter differential non-linearity (Wilhelm et al., 1997; Lemaire, private communication). This gives us the possibility to check if an image was corrected or not, simply by comparing a power spectrum of the averaged image along the slit before and after the flat field correction. The disappearance of the peak at period 2 is a clear signature of a proper flat field correction. In Fig. 2 we show the power spectrum for one of the images related to the quiet Sun before and after the subtraction with the flat field taken on 21 February 1996. The disappearance of the peak at period 2 is evident.

Judge et al., (1998) find that there is a drift in the fixed pattern of the detector with time. They quantify this drift as  $\sim 0.5$  pixel month<sup>-1</sup> in the spectral direction and 1 pixel month<sup>-1</sup> in the spatial direction. Two flat fields, taken on 21 and 28 February are available for our dataset. A cross-correlation between them reveals a drift of 0.1 pixel in the spectral direction and 0.03 in the spatial. The two flat fields are 7.5 days apart and the 21 February one is  $\sim 2.8$  days from our dataset. Assuming a linear drift, we obtain a drift of 0.037 pixels in the spectral dimension and 0.011 pixels in the spatial. We checked this result using a spectrum of the QS obtained around 856 Å. At this wavelength the continuum is particularly high and there are, practically, no spectral lines present. Instead of dividing by the average along the slit, we perform a low order fit to this average and divided each column of the image by the fit. This allows us to remove only the large scale intensity variations. The resultant image clearly shows the flat field pattern. A cross correlation between

this “artificial” flat and the 21th February flat field gives us drift values that are substantially identical to the ones obtained assuming a linear drift between the two consecutive flat fields. It is also interesting to note that if a new flat is obtained from the 21th February data in the position of the 28th February one (i.e. correcting for the spectral and spatial drift of 0.1 and 0.03 calculated above) and a new cross correlation is performed, a drift of 0.024 pixel in the spectral direction and 0.025 in the spatial ones is still present. This can be considered as a lower limit to the determination of the drift between the two images. These values are very close to the ones that we have calculated for the drift between our data and the flat field of 21th February. Drifts of 0.037 and 0.011 pixels correspond to  $\sim 0.4$  km s<sup>-1</sup> and  $\sim 0.1$  km s<sup>-1</sup> at 1250 Å. These errors are however, much smaller than the residual errors in the geometrical distortion correction (see below) and can be ignored.

### 3.3. Geometrical distortion

The electronic design of the instrument induces a geometrical distortion in the images produced by SUMER (Wilhelm et al., 1997). This effect was corrected using the routine written by T. Moran. Peter (1999), Peter & Judge (1999) and Judge et al. (1998) stress that the geometrical correction routine leaves a residual wavelength error that has a maximum value of  $\sim 0.2$  pixel. We adopt an error of 0.15 pixel taking into account these residual effects. This corresponds to an error of  $\sim 1.5$  km s<sup>-1</sup> around 1250 Å.

## 4. Data analysis

Particular attention needs to be paid to the problem of the wavelength calibration. For SUMER there is no on-board calibration source, so the wavelength calibration is done using some chromospheric lines of neutral atoms. These lines are formed in the

chromosphere at temperatures around 6500 K (e.g. Si I and S I, Chae et al., 1998a) and are supposed to be at rest (Samain, 1991). These should therefore allow the determination of an absolute wavelength scale. It is important to remember that all the absolute velocity measurements made with SUMER will be relative to these chromospheric reference lines. Lines such as C I, O I and Fe II are formed at temperatures higher than S I and Si I, (Chae et al., 1998a) and can present a certain amount of Doppler shift. Chae et al. (1998a) found redshifts of 1.5, 1.8 and 1.8 km s<sup>-1</sup> for C I, O I and Fe II respectively. Hassler et al. (1991), using the LASP EUV Coronal spectrometer on a sounding rocket flight, found a redshift of 2.7 km s<sup>-1</sup> for Fe II 1563.790. Thus, this amount of Doppler shift should be taken in account before using these lines as zero-point reference lines. Chromospheric lines disappear below 900 Å, reducing the wavelength range in which it is possible to make an absolute measure of velocity, to 900–1600 Å (first order); but, when observations are carried out in first order, some strong second order lines are recorded. In Fig. 3 we have an example of the first order spectra of NOAA 7946. It is possible to see some second order lines superimposed to the first order ones as well as chromospheric lines used for wavelength calibration.

For every image we find a preliminary wavelength scale using the information contained in the header (dispersion and wavelength of reference pixel). This is used as a starting point for the identification of the spectral lines present in the spectra. The identification of ionic lines was carried out by over-plotting the SUMER spectrum with a synthetic one, generated (for both orders) by the CHIANTI database (Dere et al., 1996, 1997). Lists of lines observed on the Sun (on disk and off disk) are available in the literature (Kink et al., 1997; Curdt et al., 1997; Feldman et al., 1997; Sandlin et al., 1986; Noyes et al., 1985; Cohen et al., 1978; Vernazza & Reeves, 1978). For laboratory wavelengths of UV spectral lines, a large dataset can be found in the literature (Kelly, 1982, 1985, 1987) and on the Internet (Harvard-Smithsonian Center for Astrophysics Databases<sup>1</sup>; National Institute of Standard and Technology on-line energy level database).

Brynildsen et al. (1998) have examined some SUMER and CDS images producing velocity maps (absolute for SUMER data and relative to the average velocity for CDS) in which they show an evident correlation between the observed redshift and the intensity of the line. Compared to the average wavelength position there is a tendency for the wavelength of the lines to change from blueshift to redshift as the peak intensity increases. This means that the redshift phenomenon is of a statistical nature, with strong local variations in the observed Doppler shift in all the TR lines. This last point is particularly important if we want to measure the average redshift. In fact, if a simple average (along the slit or over a whole image) is made, the locations with most redshift will also be the most “intense” and the averaged value will be shifted towards more red shifted values. To avoid this, it is necessary to take some precautions. Chae et al. (1998a), performed a weighted average along the slit, i.e.

they normalize the line profile by the integrated intensity before an average is taken. Brynildsen et al. (1998), calculated the shift in every position along the slit and, afterward they perform the average along the slit. The last authors showed that the values obtained in this way are systematically lower than the ones obtained with a simple average, especially in active regions. It is also interesting to underline that they found practically no differential velocity between active and quiet regions, but this difference is present when they perform a simple average (with a maximum value around 5 km s<sup>-1</sup> in O V). We have adopted the idea of Chae et al., (1998a) but we have, also, performed an average on the values calculated for every single spatial pixel (see Sect. 5.9.2) for some spectra with very high signal-to-noise ratios. We find no relevant difference between the two methods, so a weighted average along the slit was performed in order to obtain the final spectral profile to be analysed.

The measurement of the central line position, together with amplitude and full width half maximum, was performed using the Genetic Algorithm (GA) of Charbonneau (1995). A complete examination of the reliability of GA with respect to other algorithms was performed by McIntosh et al. (1998). An estimation of the errors in the derived parameters was obtained using the GA-derived parameters as input for a “classical” IDL-CURVEFIT procedure (Peter, 1999; Peter and Judge, 1999). For each spectral region of interest, we have calculated the local spectral dispersion using chromospheric lines. The formation temperatures are obtained using the data tables of the Arcetri Spectral Code (Landi & Landini, 1999; Landini & Monsignori Fossi (1990) and are listed in Table 3.

For each region of interest the dispersion relation was calculated performing a first order polynomial fit to the pairs central pixel - laboratory wavelength of the reference lines. The derived dispersion values are reported in Table 2. Generally the laboratory wavelengths of chromospheric lines are well known, with errors much less than 1 km s<sup>-1</sup>. Unfortunately this is not the case for some ionic lines (especially coronal ones) in which the errors can raise up to 1–10 km s<sup>-1</sup>. Errors in the determination of the velocity along the line of sight were hence determined considering a quadratic sum of the errors due to the Gaussian fit and to the residual errors in the geometric calibration. These results, together with the measured value are reported in Table 3. For each spectral line analysed, we measure the FWHM and, using Eq. 1, the non-thermal velocity. However, opacity effects, especially in the active region, can be important.

Chae et al. (1998b) evaluated the opacity of many spectral lines finding that the C I 1315.918, O I 1355.5977 and N I 1319.6770 are optically thin; while C II 1036 & 1037 are optically thick. Also lines due to Fe II and Si II are believed to be optically thick (Chae et al., 1998b). We are interested in the general trend of the non-thermal velocity with the formation temperature in correspondence with the trend of the Doppler shift. For this reason, we will not include non-thermal velocity values obtained for lines affected by opacity in the figures (see Figs. 9, 10, 11 lower panels later). It is also important to underline that spectral profiles are obtained doing an average along the slit, that means summing up many profiles that may have

<sup>1</sup> <http://cfa-www.harvard.edu/amp/data/amdata.html>

different central positions. This can lead to an extra broadening of the final line, particularly for narrow lines (such as C I and O I). For the narrow C I 1315.918 and O I 1355.5977 lines we evaluate the FWHM by performing an average over groups of 3 pixels along the slit for the active region dataset (over 5 for the quiet Sun). The final FWHM is an average of all the dataset. We note that FWHMs obtained by such a method are only slightly narrower ( $\sim 0.05$  pixels) than the one obtained by performing a Gaussian fit of a profile averaged over the entire slit. For hotter (broader) lines there is no practical difference between the two methods (see Sect. 5.9.2) and the weighted average over the entire slit can be used. When we compare our quiet Sun non-thermal velocity measurements (see Fig. 10, lower panel) with Chae et al. (1998b), it shows that our values are larger for low temperature lines (below  $\text{Log } T = 4.8$ ), but are consistent at higher temperatures. This is in large part due to the different choice of the FWHM of the instrumental profile. In fact, Chae et al. (1998b) assumed that the instrumental broadening can be considered as a Gaussian with a FWHM of 2.3 pixels. We used the correction package provided in the SUMER software tree, which is equivalent to a correction with a Gaussian having a FWHM of 1.92 pixels (for the  $1''$  slit on detector A). This different assumption yields larger values of non-thermal velocities especially for the narrower and cooler lines, with a difference of  $\sim 3.4 \text{ km s}^{-1}$  and  $\sim 2.3 \text{ km s}^{-1}$  for the C I 1315.918 and O I 1355.5977 lines respectively. The difference reduce to  $\sim 0.6 \text{ km s}^{-1}$  for the C IV 1548 line. It is also important to stress that, due to the non-linear dependence of the non-thermal velocity with the measured FWHM (see Eq. 1) the difference increases with the reduction of the observed FWHM, so that a small difference in the latter quantity can lead (for narrow lines) to much larger values of non-thermal velocity when a narrower instrumental profile is adopted.

## 5. Results

We have analyzed a series of spectra in several wavelength bands to measure the Doppler shifts and non-thermal velocities for quiet Sun and active regions separately. We now describe measurements of these quantities in a series of selected wavelength bands in detail. The results are depicted (in a summarized form) in Figs. 9 & 10. The readers are encouraged to refer to these two figures while reading each subsection.

### 5.1. 1560–1590 Å

Seven Fe II lines were identified in this spectral region. Five were already reported by Brekke et al. (1997). The other two lines (Fe II 1571.137 and Fe II 1581.270) were observed by Sandlin et al. (1986). All laboratory wavelengths for iron are from Kelly (1985). In this same region there are also three Si I lines at 1569.3185, 1571.4058 and 1571.796 Å (Sandlin et al. 1986; wavelengths from Kelly, 1982). In this spectral range it is possible to observe the S V 786.470 and the O IV 790.199 lines. For the S V line we have in the literature two values for the laboratory wavelength, 786.480 (Kelly, 1982) and 786.470 (Kaufman

**Table 2.** Dispersion values for different spectral regions as measured in the Quiet Sun and in an Active Region. Wavelengths for Iron are from Kelly (1985), all the others from Kelly (1982)

Spectral Range Å	Ref. line	Disp. (Å/pix)
1560–1590 (AR)	Fe II 1563.790	0.04166
	Fe II 1569.674	
	S V	
	Fe II 1571.137	
	O IV	
1540–1570 (AR)	Fe II 1571.137	0.04176
	Fe II 1581.270	
	Fe II 1584.952	
	Fe II 1588.290	
	C IV	
1520–1550 (QS)	Fe II 1550.274	0.04180
	Fe II 1559.085	
	Fe II 1563.790	
Ne VIII	Fe II 1569.674	0.04257
	C I 1542.1766	
1380–1405 (AR)	Fe II 1570.244	0.04266
	Fe II 1571.137	
	Fe II 1571.137	
	Fe II 1570.244	
1350–1365 (AR)	Si II 1526.7076	0.04180
	Si II 1533.4320	
	Ne VIII	
	C I 1542.1766	
1380–1405 (AR)	Fe II 1387.219	0.04257
	Fe II 1392.149	
	O IV	
	Si IV	
	Ar VIII	
1350–1365 (AR)	Fe II 1392.817	0.04266
	S I 1392.5878	
	C I 1354.288	
	C I 1355.844	
	Na IX	
	C I 1357.134	
	O I	
1295–1320 (AR)	C I 1357.659	0.04286
	C I 1358.188	
	C I 1359.275	
	C I 1359.438	
	C I 1364.164	
1295–1320 (AR)	S I 1295.6526	0.04286
	S I 1300.907	
	Si II	
	C I 1310.637	
	Si III	
1250–1270 (AR)	C I 1311.363	0.04296
	C I 1311.924	
	C I 1312.247	
	C I 1254.513	
	Si I 1258.795	
O V	S I 1262.8596	0.04296
	S I 1270.7821	
	S I 1270.7821	
1240–1255 (AR)	C I 1244.535	0.04307
	C I 1245.943	
	N V	
	C I 1249.004	
	Fe XII	
1025–1045 (QS)	C I 1249.405	0.04391
	C I 1252.208	
	C I 1254.513	
	O I 1027.4307	
	O I 1028.1571	
C II	O I 1039.2304	0.04391
	O I 1040.9425	
	O I 1041.6876	
O VI	O I 1040.9425	0.04391
	O I 1041.6876	
	O I 1041.6876	

& Martin, 1993). Curdt et al. (1997) using observations taken near the North Polar limb measured a wavelength of 786.470. This is consistent with Peter & Judge (1999), who has shown that the observed Doppler shift along the line of sight decrease to zero towards the solar limb. Thus the value of 786.470 will be used as the rest wavelength for S V. The value of 790.199 Å (Kelly, 1982) will be used as the rest wavelength of O IV.

### 5.1.1. Active region

Using the Fe II lines the dispersion relation was found performing a first order polynomial fit, with residuals of  $\sim 0.005$  Å. In Table 2, the lines used to find the dispersion relation are listed together with the dispersion values. With this relation the wavelengths for the Si I lines were calculated finding a total value of  $-0.4 \pm 1.1$  km s<sup>-1</sup>. Assuming the Si I lines at rest, this infers a redshift of  $0.4 \pm 1.1$  km s<sup>-1</sup> for Fe II in the Active Region. This allows us to use the Fe II lines as reference lines together with the cooler S I and Si I ones. Values of  $13.1 \pm 1.2$  km s<sup>-1</sup> and  $11.2 \pm 1.2$  km s<sup>-1</sup> were found for S V 786.470 and O IV 790.199 respectively. We also calculate the non-thermal velocity component (using Eq. 1) for Fe II, S V and O IV, finding values of  $14.1 \pm 0.2$ ,  $26.4 \pm 0.7$  and  $31.7 \pm 0.6$  km s<sup>-1</sup> respectively.

### 5.1.2. Quiet Sun

The same analysis was performed for the quiet Sun, obtaining values of  $0.0 \pm 1.6$ ,  $12.8 \pm 1.2$  and  $8.0 \pm 1.2$  km s<sup>-1</sup> for the Doppler shift of Fe II, S V and O IV, while values of  $13.9 \pm 0.6$ ,  $26.6 \pm 0.7$  and  $30.8 \pm 0.6$  km s<sup>-1</sup> were obtained for the non-thermal velocities. These values for the Doppler shift are consistent with the ones of Brekke et al. (1997) who, using the same laboratory wavelengths, obtained  $14.0 \pm 2.0$  and  $7.0 \pm 2.0$  km s<sup>-1</sup> for S V and O IV. A value of  $9.1 \pm 1.4$  km s<sup>-1</sup> for O IV 790 was found by Peter & Judge (1999).

## 5.2. 1540–1560 Å

In this spectral range the two resonance lines of C IV at 1548.195 and 1550.770 (Rottman et al., 1990) are present. The dispersion relation was found using the lines listed in Table 2. In both datasets the 1548 line shows a value for the Doppler shift  $\sim 5$  km s<sup>-1</sup> lower than the 1550 one. In our datasets the reference lines are available only up to 1550 Å. This can lead to errors in the measured shift of the 1548 line. Brekke et al. (1997) finds a difference of  $\sim 2$  km s<sup>-1</sup> between the two lines in their quiet Sun dataset.

### 5.2.1. Active region

A Doppler shift of  $10.2 \pm 1.2$  and  $14.6 \pm 1.2$  km s<sup>-1</sup> were measured for C IV 1548.195 and 1550.770 respectively, while non-thermal velocities of  $29.5 \pm 0.7$  and  $30.2 \pm 0.7$  km s<sup>-1</sup> were established for these two lines. Achour et al. (1995) found a redshift of  $13.0$  km s<sup>-1</sup> for the 1548 line using HRTS (High

Resolution Telescope and Spectrograph; Bartoe & Brueckner, 1975).

### 5.2.2. Quiet Sun

In the quiet Sun, values of  $4.9 \pm 1.2$  and  $10.7 \pm 1.2$  km s<sup>-1</sup> for the Doppler shift and  $28.4 \pm 0.7$  and  $29.5 \pm 0.7$  km s<sup>-1</sup> for the non-thermal velocities were obtained for C IV 1548.195 and 1550.770. Peter & Judge (1999) finds a value of  $4.5 \pm 1.2$  km s<sup>-1</sup> for the 1548 line, using the assumption of zero off-limb shift. Achour et al. (1995) found a value of  $6.2$  km s<sup>-1</sup> using a rest wavelength of 1548.202 Å (Kelly, 1982); that will give us a value of  $7.6$  km s<sup>-1</sup> if the laboratory wavelength of 1548.195 Å is used. Chae et al. (1998a) report an average value of  $9.6$  km s<sup>-1</sup> for C IV using rest wavelengths from Kelly (1982). Finally, Rottman et al. (1990) measured the Doppler shift for the two C IV lines along the solar equator finding a radial downflow of  $7.7 \pm 1.0$  and  $7.3 \pm 1.5$  km s<sup>-1</sup> for C IV 1548 & 1550 respectively.

## 5.3. 1520–1550 Å

In this spectral region the strong, second order, Ne VIII line at 770 Å is observed. Unfortunately the small number of reference lines make it difficult to evaluate the amount of Doppler shift showed by this line. Anyway the line centre is located at pixel 563.93 in the quiet Sun and 563.0 in the active region, while values of 595.59 (quiet Sun) and 595.45 (active region) were found for the C I 1542.1766 line (see Table 2). This lead to a “distance” of 31.7 (quiet Sun) and 32.5 (active region) pixels between the Ne VIII and the C I lines. With a dispersion of 0.0418 Å/pix this will give us a difference of  $\sim 6.5$  km s<sup>-1</sup> between the active region (more blue) and the quiet Sun. This is independent of any laboratory wavelength. For the Ne VIII laboratory wavelength the value of 770.409 Å (Bockasten et al., 1963) has been widely used in the literature (Brekke et al., 1997; Chae et al., 1998a). Recently Peter & Judge (1999) observe a *cosθ* trend in the center-to-limb Doppler shift of TR and coronal lines, that they explain in terms of prevalent mass/waves vertical motions. They also observe that the Ne VIII shows an excess of *blueshift* at disk center and, assuming that a zero shift must be observed off-limb, the authors claims a value of 770.428 Å for the rest wavelength. This value has been recently confirmed by Dammasch et al. (1999).

### 5.3.1. Quiet Sun

For the quiet Sun a redshift of  $1.8$  km s<sup>-1</sup> is found (see below) for Si II. Correcting for this value the rest wavelengths of the two Si II lines and using the C I line 1542.1766, the dispersion relation was derived. If a laboratory wavelength of 770.428 Å is assumed for Ne VIII, we find a *blueshift* of  $-1.9 \pm 2.0$  km s<sup>-1</sup>. This value is consistent with the one found by Peter & Judge (1999) of  $-2.5 \pm 1.1$  km s<sup>-1</sup> using the off-limb zero shift assumption. If the laboratory value of 770.409 Å is used instead, a redshift of  $5.5 \pm 2.0$  km s<sup>-1</sup> is obtained in very good

agreement with the value of  $5 \pm 1.5 \text{ km s}^{-1}$  (Brekke et al., 1997) and  $5.3 \text{ km s}^{-1}$  (Chae et al., 1998a) obtained using the same laboratory wavelength. A value of  $26.9 \pm 0.6 \text{ km s}^{-1}$  was found for the non-thermal velocity.

### 5.3.2. Active region

In the active region the Si II lines show a redshift of  $6.3 \text{ km s}^{-1}$ . Making the correction as outlined above, we obtain a *blueshift* of  $-7.8 \pm 2.0 \text{ km s}^{-1}$  for Ne VIII if a laboratory wavelength of  $770.428 \text{ \AA}$  is assumed, while a *blueshift* of  $-0.5 \pm 2.0 \text{ km s}^{-1}$  is obtained if the ‘older’ laboratory wavelength of  $770.409 \text{ \AA}$  is adopted. A value of  $31.1 \pm 0.6 \text{ km s}^{-1}$  was found for the non-thermal velocity.

### 5.4. 1380–1405 Å

This spectral region allows us to measure the Doppler shift of two important TR ions, two Si IV lines at  $1393.755 \text{ \AA}$  &  $1402.770 \text{ \AA}$  (Kelly, 1982) and two O IV lines at  $1399.774 \text{ \AA}$  &  $1401.156 \text{ \AA}$  (Kelly, 1982). In this wavelength range there is a second order line due to Ar VIII at  $700.245 \text{ \AA}$  (Kelly, 1982). This line is too weak to be detected in the quiet Sun, but it is strong enough in the Active region (see Fig. 3).

#### 5.4.1. Quiet Sun

In the quiet Sun redshifted values of  $10.6 \pm 1.4 \text{ km s}^{-1}$  and  $7.4 \pm 1.4 \text{ km s}^{-1}$  were found for Si IV  $1393.755 \text{ \AA}$  and  $1402.770 \text{ \AA}$  together with non-thermal velocities of  $27.3 \pm 0.8 \text{ km s}^{-1}$  and  $27.4 \pm 0.8 \text{ km s}^{-1}$  respectively. The Doppler shift value for the 1402 line is consistent with that of Brekke et al., (1997), i.e.  $7.0 \pm 2.0 \text{ km s}^{-1}$ . Chae et al. (1998a) found an average value of  $7.8 \text{ km s}^{-1}$  for Si IV. Peter & Judge find values of  $6.5 \pm 1.1$  and  $4.8 \pm 1.1 \text{ km s}^{-1}$  for Si IV  $1393.755 \text{ \AA}$  and  $1402.770 \text{ \AA}$  respectively.

For the O IV  $1399.774 \text{ \AA}$  &  $1401.156 \text{ \AA}$  lines we find redshifted values of  $10.4 \pm 1.6$  and  $8.6 \pm 1.4 \text{ km s}^{-1}$  with non-thermal velocities of  $23.1 \pm 1.3$  and  $25.8 \pm 0.8 \text{ km s}^{-1}$ . In the literature, the following values are available for the  $1401.156 \text{ \AA}$  line:  $12.0 \pm 1.6 \text{ km s}^{-1}$  (Peter & Judge, 1999),  $12 \pm 2 \text{ km s}^{-1}$  (Brekke et al., 1997) and  $10.5 \text{ km s}^{-1}$  (Achour et al., 1995), while Chae et al. (1998a) gives an averaged value of  $11 \text{ km s}^{-1}$  for O IV.

#### 5.4.2. Active region

Doppler shifts of  $15.6 \pm 1.4$  and  $15.9 \pm 1.4 \text{ km s}^{-1}$  were found for Si IV  $1393.755 \text{ \AA}$  &  $1402.770 \text{ \AA}$  together with non-thermal velocities of  $27.8 \pm 0.8$  and  $27.5 \pm 0.7 \text{ km s}^{-1}$  respectively, while redshifts of  $16.5 \pm 1.4$  and  $16.0 \pm 1.4 \text{ km s}^{-1}$  were measured for the O IV  $1399.774 \text{ \AA}$  &  $1401.156 \text{ \AA}$  lines. We measure non-thermal velocities of  $26.2 \pm 0.8 \text{ km s}^{-1}$  for the former and  $25.4 \pm 0.7 \text{ km s}^{-1}$  for the latter O IV line. Achour et al. (1995) report a value of  $17.6 \text{ km s}^{-1}$  for the O IV line at  $1401.156 \text{ \AA}$ .

In this spectral region there is a second order spectral line at  $700.245 \text{ \AA}$  due to Ar VIII. Curdt et al. (1997), report the presence

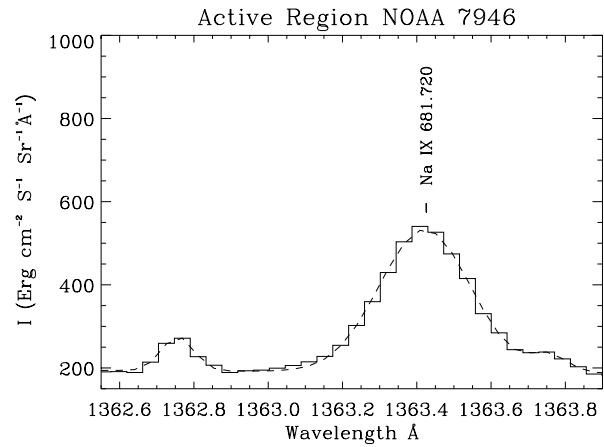


Fig. 4. Line fitting for the second order Na IX line at  $681.720 \text{ \AA}$ .

of two second order S III lines at  $700.15 \text{ \AA}$  and  $700.29 \text{ \AA}$ . We find that the line is well fitted with only one Gaussian obtaining a value of  $4.3 \pm 1.6 \text{ km s}^{-1}$ . The line shows a non-thermal velocity of  $26.0 \pm 1.4 \text{ km s}^{-1}$ .

### 5.5. 1350–1365 Å

Eight C I lines are available (see Table 2) giving us a good wavelength calibration. This region allows us to measure the Doppler shift of two O I lines at  $1355.5977 \text{ \AA}$  &  $1358.5123 \text{ \AA}$  (Kelly, 1982). A measurement of the non-thermal velocity of O I was performed using the optically thin line at  $1355.5977 \text{ \AA}$ . In this region there is also a second order line at  $681.720 \text{ \AA}$  (Kelly 1982) due to Na IX. This feature is too weak to be analyzed in the quiet Sun, but it is strong enough in the Active region to allow us a measurement of the line parameters.

#### 5.5.1. Quiet Sun

We obtain shifts of  $-0.1 \pm 1.4$  and  $1.3 \pm 1.4 \text{ km s}^{-1}$  for O I  $1355.5977 \text{ \AA}$  &  $1358.5123 \text{ \AA}$  respectively. Achour et al. (1995) found a redshift of  $0.5 \text{ km s}^{-1}$  for the O I  $1302.1685 \text{ \AA}$  line, while Chae et al. (1998a) report a value of  $1.8 \text{ km s}^{-1}$  for the same line. Finally Brekke et al. (1997) assumed no relevant shift for the O I. A non-thermal velocity of  $13.1 \pm 0.3 \text{ km s}^{-1}$  was found for the O I  $1355 \text{ \AA}$  line.

#### 5.5.2. Active region

In the Active region we measure Doppler shifts of  $1.0 \pm 1.4 \text{ km s}^{-1}$  and  $1.1 \pm 1.4 \text{ km s}^{-1}$  for the O I  $1355.5977 \text{ \AA}$  and O I  $1358.5123 \text{ \AA}$  lines respectively, while a non-thermal velocity of  $12.4 \pm 0.2 \text{ km s}^{-1}$  is measured for the optically thin O I  $1355 \text{ \AA}$  line. These values of Doppler shift are in agreement with the value of  $1.2 \text{ km s}^{-1}$  by Achour et al. (1995) for O I  $1302.1685 \text{ \AA}$ .

Curdt et al. (1997) report a S III line at  $681.50 \text{ \AA}$  that could affect the measurements of the second order line due to Na IX at  $681.720 \text{ \AA}$ . However, we are able to fit the line with only one

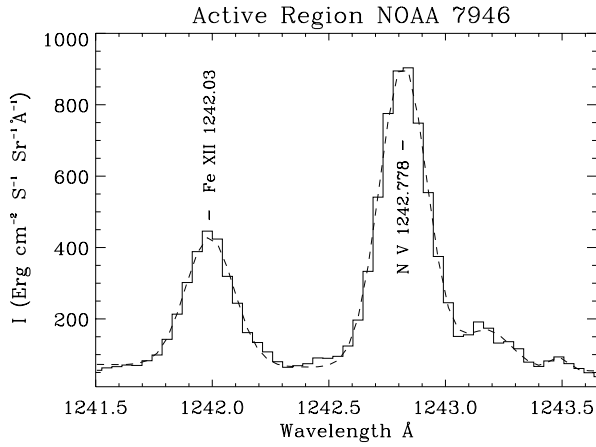


**Fig. 5.** Line fitting for the Fe XII line at 1242.03 Å.

Gaussian (see Fig. 4). We find a *blueshift* of  $-3.6 \pm 1.4 \text{ km s}^{-1}$  and a non-thermal velocity of  $27.7 \pm 0.7 \text{ km s}^{-1}$ .

### 5.6. 1295–1320 Å

Inside this spectral range numerous chromospheric lines are present. Besides the ones showed in Table 2, there are three O I lines at 1302.1685, 1304.8576 and 1306.0286 Å together with a C I line at 1315.918 Å and a N I line at 1319.6760 Å (wavelengths from Kelly 1982). Finally a Si II line at 1304.3720 Å and a Si III line at 1301.146 Å (Kelly 1982) are present. Unfortunately the latter one is blended with the S I 1300.907 Å line and only in the Active Region were we able to safely resolve the two lines.

#### 5.6.1. Active region

In the Active Region we used the lines listed in Table 2 in order to obtain the wavelength calibration. We have also checked the absence of shift between the S I and the C I lines. Using these six lines we obtain a redshift of  $6.3 \pm 1.5 \text{ km s}^{-1}$  and a non-thermal velocity of  $23.1 \pm 0.8 \text{ km s}^{-1}$  for Si II 1304.3720 Å. For Si III 1301.146 Å a redshift of  $10.1 \pm 1.5 \text{ km s}^{-1}$  and a non-thermal velocity of  $30.8 \pm 0.9 \text{ km s}^{-1}$  were obtained. Achour et al. (1995) obtained a value of  $3.8 \text{ km s}^{-1}$  for the Si II 1533.432 Å line shift. We also measure the redshift values of the three O I lines, obtaining values of  $1.0 \pm 1.5 \text{ km s}^{-1}$ ,  $1.7 \pm 1.5 \text{ km s}^{-1}$  and  $1.2 \pm 1.5 \text{ km s}^{-1}$  for the 1302, 1304 and 1306 line respectively. This result is fully consistent with that obtained in the previous spectral region. Non-thermal velocities for the optically thin line due to C I 1315.918 Å was measured, obtaining a value of  $10.2 \pm 0.6 \text{ km s}^{-1}$ .

#### 5.6.2. Quiet Sun

In the quiet Sun some of the chromospheric lines listed in Table 3 are too weak, so we used the three O I lines. A Doppler shift of  $1.2 \pm 1.5 \text{ km s}^{-1}$  was found for Si II 1304.3720 Å together with a non-thermal velocity of  $19.7 \pm 0.8 \text{ km s}^{-1}$ .

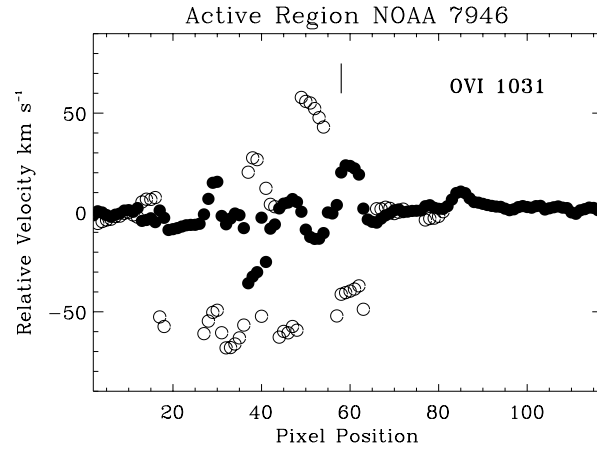


**Fig. 6.** Doppler shift of the rest component (filled circles) and of the secondary component (open circles) with respect to the average position of the rest (or primary) component. The vertical mark indicates the position along the slit of the spectral profile fitted in Fig. 7.

Adding  $0.6 \text{ km s}^{-1}$  to the value found by taking in account the measured average redshift showed by O I in the quiet Sun, we obtain a redshift of  $1.8 \pm 1.5 \text{ km s}^{-1}$ . Chae et al. (1998a) report a value of  $2.6 \text{ km s}^{-1}$  for the Si II 1260.412 Å line, while Achour et al. (1995) find a value of  $1.8 \text{ km s}^{-1}$  for the Si II 1533.432 Å line. Non-thermal velocities for optically thin lines due to C I 1315.918 Å was measured, obtaining a value of  $9.6 \pm 0.7 \text{ km s}^{-1}$ .

### 5.7. 1250–1270 Å

In this spectral region the second order O V 629.730 Å (Kelly 1982) line is present. This line is blended with a relatively strong S II 1259.530 Å line (Brekke et al. 1997, Chae et al., 1998a). The first authors observed the line in the KBr part of the detector, which suggested O V to be approximately six times stronger than the S II line. Measuring the total intensity (in count/sec) of the unresolved line in the bare and KBr parts of the detector and knowing (from the calibration curves) the ratio between the peak intensities of each line in the two different parts of the detector, it is possible to estimate (from the knowledge of the FWHM of each line) the ratio between the intensities in the bare and in the KBr part of the detector. An estimation of the FWHM can be obtained using Eq. 1. Assuming a non-thermal velocity of  $15 \text{ km s}^{-1}$  for S II and  $28 \text{ km s}^{-1}$  for O V (Chae et al., 1998b) it is possible to estimate that the O V is  $\sim 3$  times stronger than the S II in the KBr part of the detector. In the bare part this ratio rises to  $\sim 22$ , essentially due to the reduced sensitivity of the bare part at wavelengths around 1250 Å with respect to the KBr. We have therefore performed our measurements in the bare part of the detector. Performing a constrained two Gaussian fit we found that there is no substantial difference in the central position with respect to a single Gaussian fit, that we have finally used.

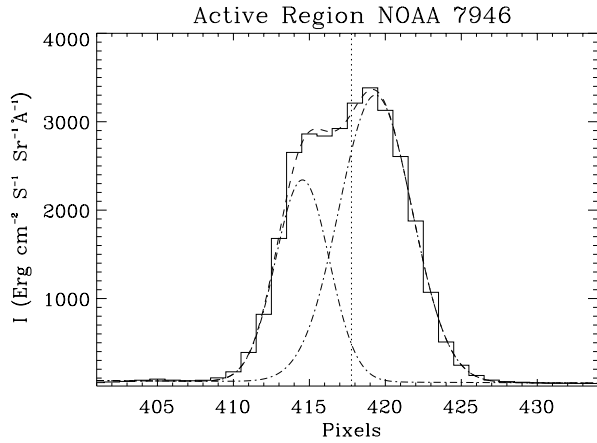


**Fig. 7.** Line fitting to the O VI line profile in the position showed in Fig. 6. The vertical dotted line represents the average central position of the rest component.

### 5.7.1. Quiet Sun

A redshift of  $7.0 \pm 1.5 \text{ km s}^{-1}$  was found together with a non-thermal velocity of  $28.5 \pm 0.8 \text{ km s}^{-1}$ . Peter & Judge (1999) find a Doppler shift of  $9.8 \pm 1.0 \text{ km s}^{-1}$ . Brekke et al. (1997) find a value of  $16.0 \pm 3 \text{ km s}^{-1}$ . However we find that the S II line is, in the KBr part, quite strong and, probably, having a larger rest wavelength than the O V line, leads to the high redshift observed by the last authors. Chae et al. (1998a), find a value of  $10.6 \text{ km s}^{-1}$ . Achour et al. (1995), found a value of  $9.0 \text{ km s}^{-1}$  for the O V 1371.292 Å line.

### 5.7.2. Active region

In the Active Region a Doppler shift of  $7.9 \pm 1.5 \text{ km s}^{-1}$  and a non-thermal velocity of  $29.1 \pm 0.8 \text{ km s}^{-1}$  were found for the O V 629.730 Å line. Achour et al. (1995), found a value of  $9.0 \text{ km s}^{-1}$  for the O V 1371.292 Å line.

### 5.8. 1240–1255 Å

In this spectral range we observe the N V 1242.778 Å (Edlén, 1934) and the Fe XII 1242.03 Å (Kelly, 1985) lines. The latter line is too weak to be reliably measured in the quiet Sun. However it is strong enough to be measured in the Active region (see Fig. 5). For the N V 1242 line, Kelly (1982) reported a rest wavelength of 1242.804 Å. However, when this rest wavelength is used, Achour et al. (1995) and Brekke et al. (1997) found too small values of redshifts with respect to the other lines formed at similar temperature. In contrast with this, Chae et al. (1998a) found an average redshift of  $11.3 \text{ km s}^{-1}$  in the quiet Sun using the laboratory wavelengths from Kelly (1982).

#### 5.8.1. Quiet Sun

A redshift of  $9.8 \pm 1.6 \text{ km s}^{-1}$  and a non-thermal velocity of  $24.9 \pm 0.8 \text{ km s}^{-1}$  were found for the N V 1242.778 Å line. Using this rest wavelength, Achour et al. (1995) found a redshift

of  $8.3 \text{ km s}^{-1}$  while Brekke et al. (1997) obtained a value of  $11.0 \pm 1.5 \text{ km s}^{-1}$ . A Doppler shift of  $9.9 \pm 1.0 \text{ km s}^{-1}$  was found by Peter & Judge (1999).

#### 5.8.2. Active region

In the active region the N V 1242.778 Å line is shifted toward the red by  $10.6 \pm 1.6 \text{ km s}^{-1}$  and shows a non-thermal velocity of  $29.4 \pm 0.8 \text{ km s}^{-1}$ . We fitted the Fe XII line with only one Gaussian (see Fig. 5), measuring a blueshift of  $-9.8 \pm 1.6 \text{ km s}^{-1}$  together with a non-thermal velocity of  $26.7 \pm 0.7 \text{ km s}^{-1}$ , although Brekke et al. (1997) report blending with S I 1241.905 Å. It is interesting to note here the SKYLAB observation by Sandlin et al. (1977) from Fe XII 1349 of a blueshift of  $-6 \text{ km s}^{-1}$ .

### 5.9. 1025–1045 Å

In this region we find two O VI 1031.9261 & 1037.6167 Å (Kaufman & Martin, 1989) and two C II 1036.3367 1037.0182 (Kaufman & Edlén, 1974) lines. The wavelength calibration was obtained using the five O I lines listed in Table 2. A value of  $0.6 \text{ km s}^{-1}$  was added to the shift values found in the quiet Sun by taking in account the O I observed redshift.

#### 5.9.1. Active region

Unfortunately, the active region spectrum is somewhat incomplete (probably due to telemetry problems) starting from pixel 548, missing part of the O VI 1037.6167 Å and the three O I lines at 1039, 1040 and 1041 Å (see Table 2.). Moreover, the two remaining O I lines (1027.4307 1028.1571 Å) appear in this active region spectrum, heavily blended with others lines (accordingly to the CHIANTI database, Fe X 1027.65 and Fe X 1028.39 Å; Curdt et al. 1997 and Hassler et al. 1997, report a Fe X at 1028.04 Å). For these reasons, we are unable to do a reliable fit of these two O I lines, making impossible the wavelength calibration of the active region spectrum. Nevertheless, it is still possible to obtain information from the O VI 1031.9261 Å line. Looking at the spectral line obtained with the weighted average along the slit, a non-Gaussian profile is immediately evident. Due to the very high intensity of this line in active regions (see Fig. 7) it is possible to perform a multi-Gaussian fit for every single spatial pixel. In many positions a two Gaussian fit was clearly necessary (see Figs. 6 & 7), showing clear evidence for shifts up to  $\pm 50 \text{ km s}^{-1}$  of the secondary component (open circles in Fig. 6) with respect to the rest component (filled circles). Doppler shifts are measured with respect to the average position of the rest component (pixel position 417.77). Explosive events are observed in mid (C IV & Si IV) and in the upper (O VI) transition region (Innes et al., 1997; Pérez et al., 1999). Our data do not have temporal resolution, but we can see many different events registered in our spectra (see Fig. 6) with an average spatial dimension of 6–7 pixels (4300–5000 km). We do not observe such clear signature of explosive events in any other UV line in the Active Region dataset. This further suggests that

**Table 3.** Doppler shifts and non-thermal velocities in the Active Region NOAA 7946 and in the Quiet Sun.

Ion	$\lambda_{lab}$ Å	$\lambda_{obs}$ Å	Log T (K)	Velocity (km/s)		$\xi$ (km/s)		Ref.
				AR	QS	AR	QS	
C I	(8 lines)	—	4.11	$0.0 \pm 1.5$	$0.0 \pm 1.5$	— —	— —	K
C I	1315.918	—	4.11	— —	— —	$10.2 \pm 0.6$	$9.6 \pm 0.7$	K
Fe II <sup>a</sup>	(7 lines)	—	4.23	$0.4 \pm 1.1$	$0.0 \pm 1.6$	$14.1 \pm 0.2$	$13.9 \pm 0.6$	K
Si II <sup>a</sup>	1304.3720	1304.3771 (QS)	4.26	$6.3 \pm 1.5$	$1.8 \pm 1.5$	$23.1 \pm 0.8$	$19.7 \pm 0.8$	K
O I	1355.5977	1355.5971 (QS)	4.31	$1.0 \pm 1.4$	$-0.1 \pm 1.4$	$12.4 \pm 0.2$	$13.1 \pm 0.3$	K
O I	1358.5123	1358.5180 (QS)	4.31	$1.1 \pm 1.4$	$1.3 \pm 1.4$	— —	— —	K
C II <sup>a</sup>	1036.3367	1036.3460 (QS)	4.71	— —	$3.3 \pm 1.9$	— —	$24.3 \pm 0.9$	KE
C II <sup>a</sup>	1037.0182	1037.0343 (QS)	4.71	— —	$5.3 \pm 1.9$	— —	$27.6 \pm 1.0$	KE
Si III	1301.146	1301.190 (AR)	4.78	$10.1 \pm 1.5$	— —	$30.8 \pm 0.9$	— —	K
Si IV	1393.755	1393.804 (QS)	4.84	$15.6 \pm 1.4$	$10.6 \pm 1.4$	$27.8 \pm 0.8$	$27.3 \pm 0.8$	K
Si IV	1402.770	1402.805 (QS)	4.84	$15.9 \pm 1.4$	$7.4 \pm 1.4$	$27.5 \pm 0.7$	$27.4 \pm 0.8$	K
C IV	1548.195	1548.220 (QS)	5.01	$10.2 \pm 1.2$	$4.9 \pm 1.2$	$29.5 \pm 0.7$	$28.4 \pm 0.7$	R
C IV	1550.770	1550.825 (QS)	5.01	$14.6 \pm 1.2$	$10.7 \pm 1.2$	$30.2 \pm 0.7$	$29.5 \pm 0.7$	R
O IV	1399.774	1399.823 (QS)	5.23	$16.5 \pm 1.4$	$10.4 \pm 1.6$	$26.2 \pm 0.8$	$23.1 \pm 1.3$	K
O IV	1401.156	1401.197 (QS)	5.23	$16.0 \pm 1.4$	$8.7 \pm 1.4$	$25.4 \pm 0.7$	$25.8 \pm 0.8$	K
N V	1242.778	1242.819 (QS)	5.25	$10.6 \pm 1.6$	$9.8 \pm 1.6$	$29.4 \pm 0.8$	$24.9 \pm 0.8$	E
S V	786.470	786.504 (QS)	5.26	$13.1 \pm 1.2$	$12.8 \pm 1.2$	$26.4 \pm 0.7$	$26.6 \pm 0.7$	KM2
O IV	790.199	790.220 (QS)	5.26	$11.2 \pm 1.2$	$8.0 \pm 1.2$	$31.7 \pm 0.6$	$30.8 \pm 0.6$	K
O V	629.730	629.745 (QS)	5.39	$7.9 \pm 1.5$	$7.0 \pm 1.5$	$29.1 \pm 0.8$	$28.5 \pm 0.8$	K
O VI	1031.9261	1031.9677 (QS)	5.47	— —	$12.7 \pm 1.9$	— —	$32.9 \pm 0.9$	KM1
O VI	1037.6167	1037.6446 (QS)	5.47	— —	$8.7 \pm 1.9$	— —	$31.7 \pm 0.9$	KM1
Ar VIII	700.245	700.255 (AR)	5.61	$4.3 \pm 1.6$	— —	$26.0 \pm 1.4$	— —	K
Ne VIII	770.428	770.423 (QS)	5.80	$-7.8 \pm 2.0$	$-1.9 \pm 2.0$	$31.1 \pm 0.6$	$26.9 \pm 0.6$	PJ
Na IX	681.720	681.712 (AR)	5.90	$-3.6 \pm 1.4$	— —	$27.7 \pm 0.7$	— —	K
Fe XII	1242.030	1241.990 (AR)	6.12	$-9.8 \pm 1.6$	— —	$26.7 \pm 0.7$	— —	K

References: K: Kelly (1982), KM1: Kaufman & Martin (1989), KM2: Kaufman & Martin (1993), E: Edlén (1934), KE: Kaufman & Edlén (1974), R: Rottman et al. (1990), PJ: Peter & Judge (1999).

<sup>a</sup> Lines that are believed to be affected by opacity (see Sect. 4).

frequent occurrence (and/or energy) of these events takes place at the O VI formation temperature.

### 5.9.2. Quiet Sun

In the quiet Sun a Doppler shift of  $12.7 \pm 1.9$  km s<sup>-1</sup> is found for O VI 1031.9261 Å and  $8.7 \pm 1.9$  km s<sup>-1</sup> for O VI 1037.6167, while non-thermal velocities of  $32.9 \pm 0.9$  km s<sup>-1</sup> and  $31.7 \pm 0.9$  km s<sup>-1</sup> were obtained. Doppler shift of  $3.3 \pm 1.9$  km s<sup>-1</sup> and  $5.3 \pm 1.9$  km s<sup>-1</sup> were found for the C II 1036.3367 & 1037.0182 Å lines, together with non-thermal velocities of  $24.3 \pm 0.9$  km s<sup>-1</sup> and  $27.6 \pm 1.0$  km s<sup>-1</sup> respectively. Due to the high signal-to-noise ratio it is possible to obtain the Doppler shift and the non-thermal velocity in every single pixel along the slit. In Fig. 8 we show the Doppler shift for the C II 1036.3367 & 1037.0182 Å and the O VI 1037.9261 Å lines. In the lower panel the total intensity along the slit in these three lines (solid line) and the contribution of the O VI (dashed line) and of the two C II lines (dotted lines) is shown. It is possible to see that the network structure is dominated by the O VI emission and that there is a dependence between intensity and redshift in C II and, especially, in O VI. Warren et al. (1997) report only a small dependence between intensity and redshift in these three lines. This analysis allows us to check the validity

of the weighted average along the slit in the extraction of the spectral profiles studied. The average values obtained in every single position along the slit are:  $3.5$  km s<sup>-1</sup> and  $5.5$  km s<sup>-1</sup> for C II 1036.3367 & 1037.0182 Å lines and  $8.1$  km s<sup>-1</sup> for the O VI 1037.9261 Å line; well inside the errors for the values found doing the weighted average along the slit. Also the values obtained for the non-thermal velocity are consistent with the ones obtained doing the weighted average along the slit. Warren et al. (1997) find a value of  $5 \pm 3$  km s<sup>-1</sup> for the O VI 1037.6167 Å line together with an average non-thermal velocity of  $34 \pm 3$  km s<sup>-1</sup>.

Brekke et al. (1997) found a redshift of  $5 \pm 1.5$  km s<sup>-1</sup> and  $6 \pm 1.5$  km s<sup>-1</sup> for the O VI 1031.9261 & 1037.6167 Å lines. An average value of  $8.7$  km s<sup>-1</sup> was found by Chae et al. (1998a), while Peter & Judge (1999) finds a redshift of  $5.6 \pm 1.1$  km s<sup>-1</sup> for the O VI 1038 line.

## 6. Discussion

In the present study we have measured the Doppler shifts of lines from various ions formed at different temperatures and different regions (quiet and active) in the solar atmosphere. They are listed in Table 3 and plotted in Figs. 9 & 10. Our results are different from those of previous studies done with SUMER (Brekke et al.

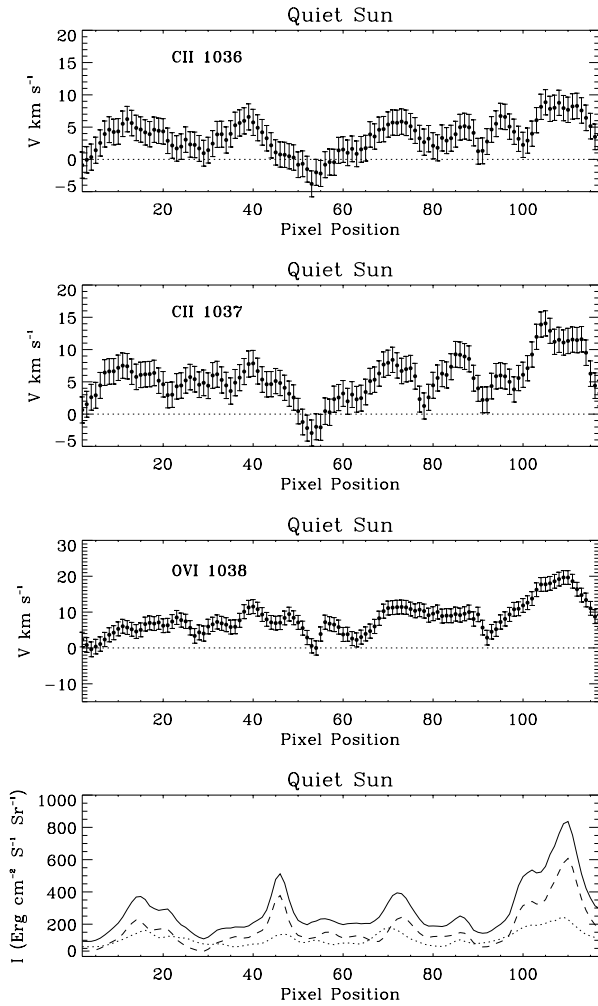


**Fig. 8.** Doppler shifts along the slit for C II 1036.3367 & 1037.0182 and O VI 1037.9261 as labeled. In the lower panel the total intensity in these three lines (solid line) in O VI (dashed line) and in the two C II lines (dotted line) are plotted.

1997; Chae et al. 1998a; Peter & Judge 1999) mainly because we have concentrated on an active region, comparing it with the quiet Sun in order to study the possible role of magnetic fields or activity on these measurements. Most of the previous studies on this problem has been done for quiet regions. Our results also includes many more UV lines and more accurate and up to date reference lines as compared to previous studies and finally we have extensively compared our results with other published work.

For active Region NOAA 7946 (top panel, Fig. 9), we find that the radial velocity is increasing from  $\sim 0 \text{ km s}^{-1}$  at  $T \sim 2 \cdot 10^4 \text{ K}$  to  $\sim 15 \text{ km s}^{-1}$  at  $T \sim 10^5 \text{ K}$  (C IV). At higher temperature the velocity is decreasing, reaching a *blueshift* of around  $-10 \text{ km s}^{-1}$  at  $T \sim 10^6 \text{ K}$ . A simple fourth order polynomial fit was applied to the data (see Fig. 9, top panel) in order to show the trend in the Active Region. From the fit it is possible to infer that the Doppler shift reversal from redshift to blueshift takes place around  $\text{Log } T = 5.7 \text{ K}$  ( $5 \cdot 10^5 \text{ K}$ ). No weights were

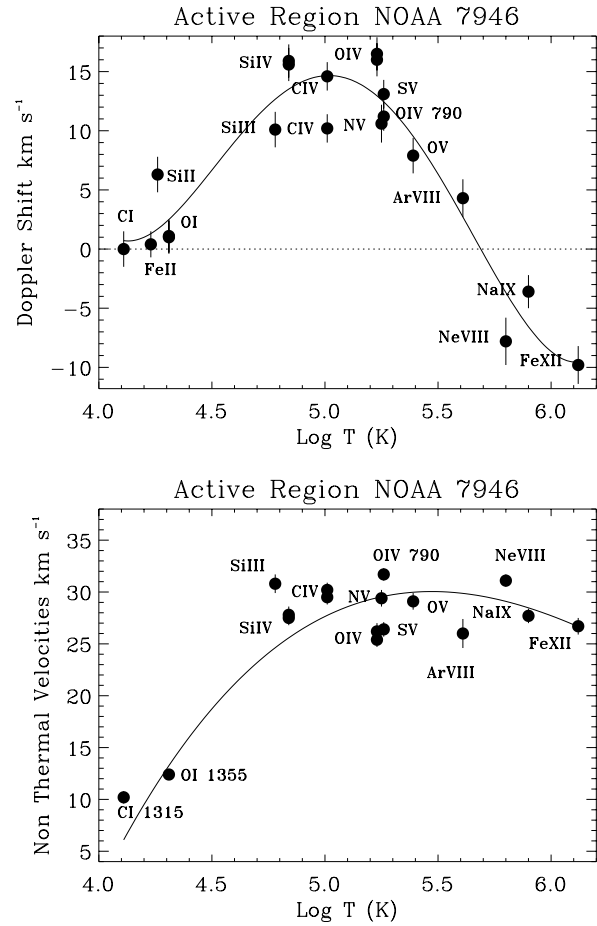


**Fig. 9.** SUMER measurement of Radial Velocities (top panel) and non-thermal velocities in Active Region NOAA 7946. Solid lines represents a simple fourth order polynomial fit (top panel) and a third order weighted polynomial fit (lower panel). Lines which are affected by opacity are not included in the lower panel (see Sect. 4).

applied to the data due to the uncertainty in the laboratory wavelengths. The behaviour at high temperature is well represented from the measurement of 4 different spectral lines (i.e. Ar VIII, Ne VIII, Na IX and Fe XII).

In the quiet Sun (see top panel of Fig. 10) we observe a slightly different trend especially at temperatures higher than  $10^5 \text{ K}$ . In fact a maximum velocity of  $\sim 10 \text{ km s}^{-1}$  is reached at  $T \sim 1.9 \cdot 10^5 \text{ K}$  (O IV, N V) and then drops down to a *blueshift* of  $-1.9 \text{ km s}^{-1}$  at the Ne VIII formation temperature ( $6.3 \cdot 10^5 \text{ K}$ ). Also in this case a simple fourth order polynomial fit was applied to the data. Due to the presence of only one high temperature line, it is more difficult to establish the temperature where the change from redshift to blueshift occur. In any case we can suggest a value between  $\text{Log } T = 5.7$  and  $\text{Log } T = 5.75$  ( $5.0 \cdot 10^5 - 5.6 \cdot 10^5 \text{ K}$ ), in agreement with Peter & Judge (1999) who find the turnover point at  $\text{Log } T = 5.7$ . From the analysis of the non-thermal velocities versus temperature distributions (see Figs. 9 & 10, lower panels) we note that both curves peak around  $\text{Log } T = 5.4$  (quiet Sun) and  $\text{Log } T = 5.5$  (Active Region), i.e. around the O VI formation temperature. These values were ob-

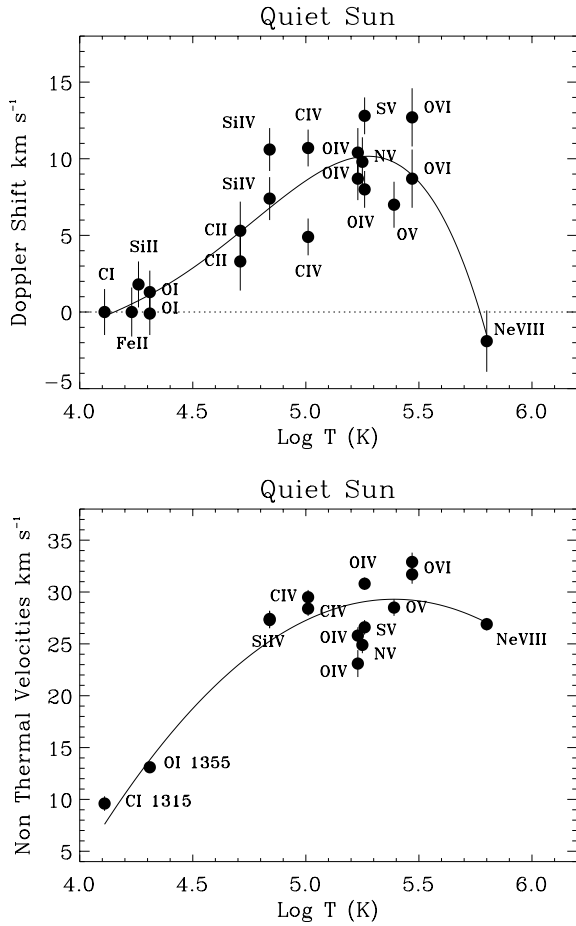


**Fig. 10.** SUMER measurement of Radial Velocities (*top panel*) and non-thermal velocities in Quiet Sun. Solid lines represents a simple fourth order polynomial fit (*top panel*) and a third order weighted polynomial fit (*lower panel*). Lines which are effected by opacity are not included in the lower panel (see Sect. 4).

tained applying a third order weighted polynomial fit to the data. The most interesting point to note here is that the O VI formation temperature is also characterized by high occurrence of explosive events (see Sect. 5.9.1, Pérez et al. 1999) that are generally not observed in higher temperature lines (Peter & Judge, 1999).

Achour et al., (1995), introduced the idea of a ‘differential redshift measurement’, i.e. to compare quiet Sun and active region Doppler shift measurement. This method has the advantage of being independent of laboratory wavelengths. They found that the differential velocity increases with increasing temperature, reaching a maximum of  $7 \text{ km s}^{-1}$  at a temperature of  $1.0\text{--}1.35 \cdot 10^5 \text{ K}$  where the N IV 1486 Å and the O IV 1401 Å lines are formed. Above this temperature the velocity difference decreases abruptly with increasing temperature. It should be noted that they did not use measurement of lines formed above  $2.4 \cdot 10^5 \text{ K}$ , so they inferred the disappearance of the differential redshift in the high transition region by extrapolating the result from the O V line. In Fig. 11 we plot our differential measurements. Our results show (see upper panel of Fig. 11) a differential velocity of  $5\text{--}7 \text{ km s}^{-1}$  around  $6.9 \cdot 10^4 \text{ K}$ , con-

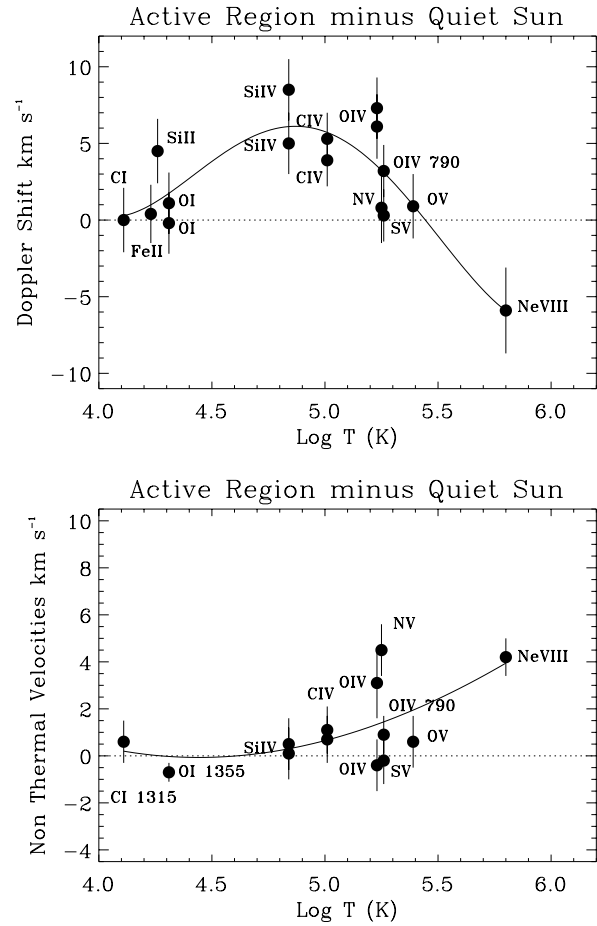


**Fig. 11.** SUMER measurement of the Differential Radial Velocities (*top panel*) and differential non-thermal velocities in Active Region NOAA 7946 minus Quiet Sun. Solid lines represents a simple fourth order polynomial fit (*top panel*) and a simple third order polynomial fit (*lower panel*).

sistent with the one observed by Achour et al. (1995). The behaviour at higher temperatures shows an opposite trend, i.e. a smaller blueshift in the quiet Sun than in the Active Region ( $\sim -6 \text{ km s}^{-1}$ ).

Our results of the temperature variations of the Doppler shifts and non-thermal velocities in the quiet Sun and active region have important implications for the validity of the physical models present for the red shift problem. There are different models present in the literature, namely return of spicular material, siphon flows through loops, nano-flares and explosive events (see Brekke et al. 1997; Peter & Judge 1999 and reference therein). Out of the all these we feel the most relevant and consistent with our observation is by Hansteen (1993). He considers nano-flares occurring at the top of coronal loops, generating MHD waves that propagate downward along the magnetic fields towards and through the transition region. This model has been extended by Hansteen et al. (1996) including the reflection that the chromosphere exerts on the downward travelling waves. Also this model predicts redshifts in the quiet Sun of  $\sim 15 \text{ km s}^{-1}$  at the C III formation temperature ( $8 \cdot 10^4 \text{ K}$ ) and

blueshifts of  $\sim -15 \text{ km s}^{-1}$  at the Mg IX formation temperature ( $10^6 \text{ K}$ ). These are too large with respect to our quiet Sun results. However, it is able (as also pointed out by Peter & Judge, 1999) to explain the presence of blueshift together with redshift within one model. Following the suggestion of Peter & Judge (1999) we support the idea of prevalent occurrence of nano-flares around the O VI formation temperature ( $3 \cdot 10^5 \text{ K}$ ) as a source for the redshift observed in the low and middle transition region and for the blueshift seen in the upper transition region and coronal lines. This can also explain the peak of the non-thermal velocity curves at the O VI formation temperature. From this point of view the larger range of values detected for the active region could be explained in terms of higher frequency of occurrence and/or energy of nano-flares events in the Active region with respect to the quiet Sun. The behaviour of the difference between the non-thermal velocity in the Active region with respect to the quiet Sun (see Fig. 11, lower panel) shows that there is an increase with increasing temperature that, again, could be explained in terms of larger energy deposition in the middle-high transition region. We hope that our results, particularly the ones for active region will shed further light into the transition region modelling. Furthermore our differential measurements provides clues for the possible role of magnetic fields in the transition region.

*Acknowledgements.* Research at Armagh Observatory is grant-aided by the Department of Education for N. Ireland while partial support for software and hardware is provided by the STARLINK Project which is funded by the UK PPARC. This work was supported by PPARC grant GR/K43315. We would like to thank the SUMER and EIT teams at Goddard Space Flight Center for their help in obtaining the data. The SUMER project is financially supported by DLR, CNES, NASA, and PRODEX. SUMER is part of SOHO, the Solar and Heliospheric Observatory of ESA and NASA. We would like to thank Scott McIntosh for a copy of his GA routine. We would also like to thank the referee Harry Warren for his comments and Werner Curdt, Philippe Lemaire & Klaus Wilhelm for helpful suggestions during the data reduction.

## References

- Achour H., Brekke P., Kjeldseth-Moe O., Maltby P., 1995, ApJ 453, 945
- Bartoe J.-D.F., Brueckner G.E., 1975, J. Opt. Soc. Am. 65, 13
- Bockasten K., Hallin R., Hughes T.P., 1963, Proc. Phys. Soc. London 81, 522
- Brekke P., Hassler D.M., Wilhelm K., 1997, Solar Phys. 175, 349
- Brynildsen N., Brekke P., Fredvik T., et al., 1998, Solar Phys. 181, 23
- Chae J., Yun H.S., Poland A.I., 1998a, ApJS 114, 151
- Chae J., Schüle U., Lemaire F., 1998b, ApJ 505, 975
- Charbonneau P., 1995, ApJS 101, 309
- Cohen L., Feldman U., Doschek G.A., 1978, ApJS 37, 393
- Curdt W., Feldman U., Laming J.M., et al., 1997, A&AS 126, 281
- Dammasch I.E., Wilhelm K., Curdt W., Hassler D.M., 1999, A&A 346, 285
- Dere K.P., Monsignori Fossi B.G., Landi E., Mason H.E., Young P.R., 1996, AAS Meeting, 188.8501
- Dere K.P., Landi E., Mason H.E., Monsignori Fossi B.G., Young P.R., 1997, A&AS 125, 149
- Doschek G.A., Feldman U., Bohlin J.D., 1976, ApJ 205, L177
- Edleń B., 1934, Nova Acta R. Soc. Sci., Uppsala (IV) 9, 6
- Feldman U., Behring W.E., Curdt W., et al., 1997, ApJS 113, 195
- Hansteen V.H., 1993, ApJ 402, 741
- Hansteen V.H., Maltby P., Malagoli A., 1996, In: Bentley R.D., Mariska J.T. (eds.) Magnetic Reconnection in the Solar Atmosphere. ASP Conference Series 111, p. 116
- Hassler D.M., Rottman G.J., Orrall F.Q., 1991, ApJ 372, 710
- Hassler D.M., Wilhelm K., Lemaire P., Schüle U., 1997, Solar Phys. 175, 375
- Hollandt J., Schüle U., Paustian W., et al., 1996, Appl. Opt. 35, 5125
- Innes D.E., Inhester B., Axford W.I., Wilhelm K., 1997, Nat 386, 811
- Judge P.G., Hansteen V., Wikstøl Ø., et al., 1998, ApJ 502, 981
- Kaufman V., Edleń B., 1974, J. Phys. Chem. Ref. Data 3, 825
- Kaufman V., Martin V.C., 1989, J. Opt. Soc. Am. 6, 1769
- Kaufman V., Martin V.C., 1993, J. Phys. Chem. Ref. Data 22, No. 2, 279
- Kelly R.L., 1982, Atomic and Ionic Spectrum Lines Below 2000 Angstroms. Oak Ridge National Laboratory, Tennessee (U.S.)
- Kelly R.L., 1985, In: Wiese W.L. (ed.) Spectroscopic Data for Iron. National Bureau of Standards (U.S.)
- Kelly R.L., 1987, J. Phys. Chem. Ref. Data 16, Suppl. No. 1
- Kink I., Jupén C., Engström L., et al., 1997, ApJ 487, 956
- Landi E., Landini M., 1999, A&AS, in press
- Landini M., Monsignori Fossi B.C., 1990, A&AS 82, 229
- Lemaire P., Wilhelm K., Curdt W., et al., 1997, Solar Phys. 170, 105
- Mariska J.T., 1992, The Solar Transition Region. Cambridge University Press, Cambridge
- McIntosh S.W., Diver D.A., Judge P.G., et al., 1998, A&AS 132, 145
- Noyes R.W., Raymond J.C., Doyle J.G., Kingston A.E., 1985, ApJ 297, 805
- Pérez M.E., Doyle J.G., Erdélyi R., Sarro L.M., 1999, A&A 342, 279
- Peter H., 1999, ApJ 516, 490
- Peter H., Judge P.G., 1999, ApJ 522, in press
- Rottman G.J., Hassler D.M., Jones M.D., Orrall F.Q., 1990, ApJ 358, 693
- Samain D., 1991, A&A 244, 217
- Sandlin G.D., Brueckner G.E., Tousey R., 1977, ApJ 214, 898
- Sandlin G.D., Bartoe J.-D.F., Brueckner G.E., 1986, ApJS 61, 801
- Siegmund O.H.W., Gummin M.A., Stock J.M., et al., 1994, Proc. SPIE 2280, 89
- Vernazza J.E., Reeves E.M., 1978, ApJS 37, 485
- Warren H.P., Mariska J.T., Wilhelm K., Lemaire P., 1997, ApJ 484, L91
- Wilhelm K., Curdt W., Marsh E., et al., 1995, Solar Phys. 162, 189
- Wilhelm K., Lemaire P., Curdt W., et al., 1997, Solar Phys. 170, 75